NASA TECHNICAL MEMORANDUM

NASA TM-73842

NASA TM-73842

(NASA-TM-73842) PREDICTED INLET GAS TEMPERATURES FOR TUNGSTEN FIBER REINFORCED SUPERALLOY TURBINE BLADES (NASA) 23 p HC A02/MF A01 CSCL 21E

N78-19157

Unclas

G3/07 08678

PREDICTED INLET GAS TEMPERATURES FOR TUNGSTEN FIBER REINFORCED SUPERALLOY TURBINE BLADES

by Edward A. Winsa, Leonard J. Westfall, and Donald W. Petrasek
Lewis Research Center
Cleveland, Ohio 44135

TECHNICAL PAPER to be presented at the
Second International Conference on Composite Materials
sponsored by the American Institute of Mining, Metallurgical, and Petroleum Engineers
Toronto, Canada, April 16-20, 1978

Abstract

Tungsten fiber reinforced superalloy composite (TFRS) impingement cooled turbine blade inlet gas temperatures were calculated taking into account material spanwise strength, thermal conductivity, material oxidation resistance, fiber-matrix interaction, and coolant flow. Measured values of TFRS thermal conductivities are presented. Calculations indicate that blades made of 30 volume percent fiber content TFRS having a 12,000 N-m/kg stress-to-density ratio while operating at 40 atmospheres and a 0.06 coolant flow ratio could permit a turbine blade inlet gas temperature of over 1900K. This is more than 150K greater than similar superalloy blades.

PREDICTED INLET GAS TEMPERATURES FOR TUNGSTEN FIBER

REINFORCED SUPERALLOY TURBINE BLADES

by Edward A. Winsa, Leonard J. Westfall, and Donald W. Petrasek

National Aeronautics and Space Administration
Lewis Research Center
Cleveland, Ohio

E-9429

Summary

Tungsten fiber reinforced superalloys (TFRS) are potentially useful as turbine blade materials because they have many desirable properties. The purpose of the present work was to predict the magnitude of the turbine inlet gas temperatures potentially achievable using first generation TFRS turbine blades, both uncoated and with thermal barrier coatings. The calculations were based on TFRS composites assuming conservative properties and a specific hypothetical blade design.

Bulk and surface metal temperature allowables were calculated for 30 and 60 volume percent fiber TFRS and MAR M200 blades operating over a range of stress-to-density ratios. The TFRS were assumed to be cross plied for transverse strength, and the strength degrading effect of fiber matrix reaction penetration was considered. The thermal conductivities of two representative TFRS were measured over a range of temperatures. Conductivities were calculated for additional fiber contents and temperatures. Cooled blade heat balance values as well as pertinent material property equations were used to calculate turbine inlet gas temperatures.

The following results were obtained. Cooled TFRS blades may allow significantly higher gas temperatures than are possible with superalloy blades. For instance, compared to a MAR M200 impingement convection cooled blade operating at 40 atmospheres, with a coolant flow of 6 percent, and having a 12,000 N-m/kg stress-to-density ratio, similar geometry 30 and 60 volume percent TFRS blades may permit 150K and 200K higher inlet gas temperatures, respectively. At high coolant flows (about 10 percent) a 60 volume percent TFRS blade could operate at a turbine inlet gas temperature of over 2100K compared to only 1850K for a similar MAR M200 blade. TFRS blades may also allow coolant flow reductions of about 45 to 65 percent when operating at the same gas temperatures and stress-to-density ratios as similar MAR M200 airfoils.

Thermal barrier coated TFRS airfoils could permit turbine inlet gas temperatures of 2100K at coolant flows below 4 percent, assuming the thermal barrier survived the temperature. The inlet gas temperatures achievable with thermal barrier coated TFRS would probably be limited by the relatively low allowable ceramic-to-bonding alloy interface temperature, which will probably be under 1400K. On the other hand, the thermal expansion of TFRS might be made to closely match that of a zirconia thermal barrier. This would be advantageous under thermal cyclic operating conditions, insofar as coating durability is concerned.

The transverse (through the wall) conductivity of TFRS blades will be about 35 to 50 W/m-K, and their longitudinal (spanwise) conductivity will be about 45 to 65 W/m-K. A typical superalloy has conductivity of approximately 25 W/m-K at 1300K. The roots of TFRS blades may be cooler during operation than the root of a similar superalloy blade because of the conductivity difference.

Introduction

Tungsten fiber reinforced superalloy composites (TFRS) are potentially useful as turbine blade materials because they have many desirable properties, such as good stress rupture and creep resistance, high modulus, good oxidation resistance, ductility, impact damage resistance, and microstructural stability (Refs. 1 through 4). Furthermore, detailed estimates indicate that finished TFRS impingement convection cooled blades could cost less than DS superalloy, DS eutectic, or oxide dispersion strengthened blades, Ref. 5.

The purpose of the present work was to predict the magnitude of turbine blade inlet gas temperatures potentially achievable using first generation TFRS turbine blades. Potential impingement convection cooled TFRS blade inlet gas temperatures are calculated and compared to those potentially possible with a similar impingement convection cooled superalloy blade. Moreover, potential inlet gas temperatures of TFRS blades coated with a zirconia thermal barrier are presented. Also presented are measured values of TFRS thermal conductivity over a range of temperatures and fiber volume fraction loadings. The measured conductivities are extrapolated to other temperatures and fiber loadings of interest using equations from the literature. Some TFRS blade design considerations are briefly discussed.

Materials, Apparatus, and Procedure

Thermal conductivity values were measured for two composites and two matrix materials to check the validity of calculations and provide a TFRS conductivity data base. The specimens and measurement procedure will be described in this section. In addition, the equations and assumptions used to calculate the conductivities and turbine blade inlet gas temperatures will be described. Also, the method of calculating TFRS metal temperature allowables will be described.

Thermal Conductivity Specimens

We measured the conductivity of four different materials in the experimental portion of this study. They were

1. Unreinforced FeCrAlY, 23 (weight percent) Cr - 5 Al - 1Y - Fe (bal.)

2. W/FeCrAlY composite, W - 1 ThO_2/FeCrAlY

3. Unreinforced ALLOY 3, 15 Cr - 25 W - 2 Al - 2 Ti - Ni (bal.)

4. W/ALLOY 3 composite, 218CS/ALLOY 3

218 CS is an unalloyed, doped tungsten lamp filament wire that has been cleaned and straightened. W - 1 ThO_2 is also an unalloyed lamp filament wire containing a dispersed oxide phase. Both wires are heavily worked.

All the composites were unidirectionally reinforced and in sheet or bar form. A typical composite sheet cross section after fabrication is shown in

Fig. 1; the bar cross sections were similar in appearance. The FeCrAlY matrix was fabricated into sheet by hot pressing layers of powder cloth as described in Ref. 6. The W/FeCrAlY composite was also fabricated into sheet but contained 50 volume percent tungsten fibers that were 0.038 cm in diameter. In both cases the sheet was about 0.13 cm thick which is approximately the wall thickness at the root of some advanced hollow turbine blade airfoils. The FeCrAlY and W/FeCrAlY sheets were cut into conductivity specimens 1.27 cm in diameter. The ALLOY 3 matrix and W/ALLOY 3 composite conductivity specimens were in the form of cylinders cut from bars. The bars had been fabricated by slip casting nickel alloy powder around he tungsten fibers and then hot isostatically pressing as described in Ref. 3. The specimens measured 1.27 cm in diameter by 0.5 cm thick. The composite specimen contained 65 volume percent tungsten fibers whose axes were parallel to the axis of the cylindrical specimen.

Thermal Conductivity Measurement

We determined the conductivity of the W/FeCrAlY in a direction perpendicular to the fiber axis (transverse) and the conductivity of the W/ALLOY 3 in a direction parallel to the fiber axis (longitudinal) using the apparatus shown in Fig. 2. We used the same apparatus to determine the conductivity of the unreinforced FeCrAlY and ALLOY 3 matrices. As shown in Fig. 2, heat passes through a thermocoupled reference coupon, then through the thermocoupled TFRS, and finally through a second thermocoupled reference coupon. The reference coupons were 0.25 cm thick by 1.27 cm in diameter stainless steel cylinders that had been carefully removed from a conductivity standard bar (Standard Reference Material 735-M1) purchased from the National Bureau of Standards. The thermocouples were welded to each side of the reference coupons and specimen.

The quantity of heat passing through each reference coupon can be calculated using the measured temperature drop across the coupon, the coupon dimensions, and the coupon conductivity. We averaged the quantities of heat passing through the two reference coupons and assumed that the average quantity also passed through the specimen between them. Taking the preceding into account, we calculated the conductivity of the composites and matrices using the measured temperature drops across the reference/specimen/reference assembly substituted into the following equation:

$$k = (Q \times d)/(S \times \Delta T) \tag{1}$$

(Refer to Appendix for symbols.) Our measurements on samples having known conductivity values were accurate within 10 percent. We believe that this accuracy is adequate to indicate trends.

Composite Conductivity Predictive Equations

According to Ref. 7, the longitudinal conductivity (conductivity measured in a direction parallel to the fibers) of unidirectional fiber reinforced composites obeys the rule of mixtures. Thus,

$$k_{\ell} = (k_f \times V_f) + (k_m \times V_m) \tag{2}$$

The transverse conductivity is not as easy to calculate. References 7 to 10 propose a variety of different calculation methods. According to the references, these methods typically produce errors between calculated and observed values of under 10 percent. We elected to use the thermal model equation from Ref. 7 because, according to the data in Ref. 7, it gives conservative estimates of the transverse conductivity for square arrays at all fiber contents, and it gives close estimates for hexagonal arrays at fiber contents under 60 volume percent. The equation is

$$k_t = k_m\left(\left[1 - 2\left(\frac{V_f}{\pi}\right)^{1/2}\right] + \frac{1}{B}\left\{\pi - \frac{4}{\left(1 - \frac{B^2V_f}{\pi}\right)^{1/2}} \tan^{-1}\frac{\left(1 - \frac{B^2V_f}{\pi}\right)^{1/2}}{\left[1 + B\left(\frac{V_f}{\pi}\right)^{1/2}\right]}\right\}\right) \quad (3)$$

$$B \equiv 2\left(\frac{k_m}{k_f} - 1\right)$$

<u>Assumed Fiber and Matrix Conductivities</u>

To use the preceding equations, one must have conductivity values for the fibers and matrices under consideration. These conductivity values will vary as a function of alloy element content, prior material history, and the temperature at which the conductivity is measured. We chose some representative conductivity values based on the following rationale:

In the case of the matrix, we chose to use heat-treated nickel-base alloy conductivity values from Ref. 11. Figure 3 depicts the range of matrix conductivity values appropriate to TFRS. The upper bound is the conductivity curve for IN600 which is the most conductive nickel base alloy under study in our laboratory for TFRS application. The lower bound is the conductivity curve for NIMONIC 80A which is the least conductive nickel base alloy matrix under study in our laboratory. In subsequent calculations, unless otherwise indicated, we used the average of the IN600 and NIMONIC 80A data. Thus, we define a typical matrix alloy to be one whose conductivity at a given temperature is given by

$$k(\text{typical}) = [k(\text{IN800}) + k(80\text{A})]/2 \quad (4)$$

We assumed that typical matrix alloys were isotropic with regard to conductivity.

The range of conductivities appropriate to TFRS are also shown in Fig. 3. The conductivity values of annealed, pure tungsten from Ref. 12 are plotted in Fig. 3 as the upper bound of the tungsten conductivity band. The conductivities of current first generation fibers, such as W - 1.0 ThO_2 and W - 1.5 ThO_2, are assumed to be given by the middle tungsten curve in Fig. 3. Experimental data to be presented later indicate that this assumption is reasonable. Consequently, all calculations with Eqs. (2) and (3) involved the use of conductivities given by the middle curve. Stronger tungsten fibers than those currently in use may have 40 percent less conductivity than annealed, pure tungsten; the resulting conductivity curve is plotted as the lower bound of the tungsten band in Fig. 3. The reasons for the lower bound are as follows. Tungsten fibers used as reinforcement are neither annealed nor pure. According to Ref. 13, modest alloying (more alloying than is used in current reinforcing fibers) can reduce annealed tungsten conductivity by 20 percent. Moreover, our measurements of the electrical conductivity (which correlates with thermal conductivity) of annealed, pure tungsten wire and worked, pure tungsten wire indicate that worked wire may have 15 percent lower conductivity than annealed wire. So, to be conservative, we subtracted 40 percent from the pure, annealed tungsten values to obtain an estimate for advanced fibers. Also, we assumed that the wire was isotropic with regard to conductivity. Actually, because reinforcing fibers have a directional microstructure, they probably are anisotropic with respect to conductivity. We believe that this will not have a significant effect, however.

Heat Balance Equations

An objective of this study was to compare the turbine inlet gas temperatures potentially obtainable using TFRS impingement convection cooled blades with those potentially obtainable using advanced-superalloy impingement convection cooled blades. We elected to compare TFRS to MAR M200 because it is one of the highest strength, high temperature turbine blade alloys in current use. Since thermal barrier coatings have shown much promise of late, Refs. 14 and 15, we made our comparisons assuming both uncoated and thermal barrier coated blades.

We used Eqs. (5) and (6) to calculate the metal and turbine inlet gas temperatures associated with the hypothetical impingement convection cooled turbine blade wall depicted in Fig. 4(a).

$$Q = \frac{T_g - T_c}{\frac{1}{h_g} + \frac{L_{III}}{K_{III}} + \frac{1}{h_c}} \tag{5}$$

$$Q = h_g(T_g - T_3) = \frac{K_{III}}{L_{III}}(T_3 - T_4) = h_c(T_4 - T_c) \tag{6}$$

We used Eqs. (7) and (8) to calculate metal and turbine inlet gas temperatures for the hypothetical thermal barrier coated impingement cooled turbine blade wall shown in Fig. 4(b).

$$Q = \frac{T_g - T_c}{\frac{1}{h_g} + \frac{L_I}{K_I} + \frac{L_{II}}{K_{II}} + \frac{L_{III}}{K_{III}} + \frac{1}{h_c}} \tag{7}$$

$$Q = h_g(T_g - T_1) = \frac{K_I}{L_I}(T_1 - T_2) = \frac{K_{II}}{L_{II}}(T_2 - T_3) = \frac{K_{III}}{L_{III}}(T_3 - T_4) = h_c(T_4 - T_c) \tag{8}$$

These equations were obtained from Ref. 14 where they were used to calculate temperatures for both uncoated and thermal barrier coated air cooled vanes. Although these equations are for the one dimensional case, a comparison of calculations using these equations with experimental data made in Ref. 14 indicated good agreement.

The assumed values of the variables needed to solve Eqs. (5) to (8) are listed in Table I. The equation for h_c in Table I is from Ref. 14 as are the values for K_I and K_{II}. The gas heat transfer coefficient values are those that would be expected in an advanced engine operating at 40 atmospheres. The nominal value of h_g is taken to be 9000 W/m-K at 2200K (Ref. 15 used 8994 W/m-K at 2200K), and it is assumed to vary with temperature as indicated in Table I. The magnitude of the temperature dependence was chosen to be similar to that indicated by Ref. 16.

Material Temperature Allowables

Use of Eqs. (5) to (8) to determine turbine inlet gas temperatures requires the definition of material temperature allowables. The cyclic oxidation and hot corrosion data in Ref. 17 indicates a maximum surface temperature allowable for a FeCrAlY matrix TFRS of about 1420K. We likewise infer from the same reference that MAR M200 coated with a conventional high quality oxidation protective coating is limited to 1350K metal surface temperature. For thermal barrier coated blades, Ref. 14 sets the maximum temperature of the zirconia-nichrome interface at 1365K. (Zirconia is the thermal barrier, and nichrome is the bond coating.)

We developed the following system of equations to obtain an estimate of TFRS blade spanwise strength (σ_a) as a function of temperature (T), time (t), and fiber volume fraction.

$$\log(\sigma_f) = A_f + B_f \times T \times (C_f + \log(t)) \tag{9}$$

$$\log(\sigma_m) = A_m + B_m \times T \times (C_m + \log(t)) \tag{10}$$

$$RP^2 = RP^2(\text{initial}) + D \times \exp(E/T) \times t \tag{11}$$

$$XPLY = 0.95 - (0.3/\sigma_m) \tag{12}$$

$$\sigma_a = V_f \times \sigma_f \times ((R - RP)/R)^2 \times XPLY \tag{13}$$

$$\rho_a = V_f \times \rho_f + V_m \times \rho_m \tag{14}$$

Equations (9) and (10) are Larson-Miller equations for unreacted fibers and matrix, respectively. Equation (11) gives the fiber-matrix reaction penetration depth. Equation (12) provides an approximate estimate of the fraction of spanwise strength remaining after cross plying. Equation (13) gives the composite blade spanwise strength. Only the unreacted fiber area is assumed to carry spanwise load; matrix and reacted fiber area are assumed to carry no spanwise loads (the matrix must carry shear loads). The spanwise strength divided by the density (Eq. (14)) gives the strength-to-density ratio. The values of the constants assumed for a typical first generation TFRS are given in Table II.

In order to obtain the values listed in Table II, we used W - 1 ThO_2/FeCrAlY composite stress rupture and fiber-matrix reaction data taken from Ref. 4. The composite stress rupture strength values were reduced by 10 percent and used with Eq. (13) (XPLY set equal to 1) to calculate apparent fiber strengths as functions of time and temperature. We fitted these calculated fiber stress rupture strengths to Eq. (9) by a least squares method. Matrix Larson-Miller parameters were selected to give strengths between those of IN600 and FeCrAlY which are the two weakest matrix alloys that we are currently studying. The reaction data from Ref. 4 were fitted to Eq. (11) by a least squares method.

Bulk metal temperature allowables for 30 and 60 volume percent TFRS and MAR M200 blades are given in Figs. 5(a) and (b). The MAR M200 allowable curve is a Larson-Miller fit of data from Ref. 11. The strength-to-density ratio allowables for TFRS were calculated using Eqs. (9) to (14) which assume a constant volume fraction fiber content along the blade span. Normally, in designing a blade an attempt would be made to vary the fiber content as a function of strength requirements along the span. This would result in a lower average fiber content in the airfoil. Because the average airfoil density would be lower, stresses would be reduced and the allowables would be higher. Since selective reinforcement is not always possible, the calculations of this investigation were made assuming constant volume fraction fiber content. Effective selective reinforcement would normally require that the airfoil span be at least two times the average fiber critical length (critical length can be approximated by $2 \times R \times \sigma_f/\sigma_m$); moreover, blade wall thickness, blade weight, and fiber-matrix reaction considerations must allow five or more plies to be used in each wall.

In this report TFRS allowables from Fig. 5(a) (0.02 cm diameter fibers) were used in calculations because small diameter fibers are more easily incorporated into the hollow aircraft size blades with which we are most concerned. However, in suitable applications (such as solid aircraft blades or larger land based turbine blades) larger diameter fibers would permit higher use temperatures than small diameter fibers as is evident in comparing Figs. 5(a) and (b). The reason for this is that the strength degradation caused by reaction between fibers and matrix is less severe as a function of time and temperature for larger fibers. Moreover, higher strength tungsten fibers (such as W-Hf-C, Ref. 2) than those used in Ref. 4 (W-1ThO_2) could permit up to 100K higher TFRS bulk temperature allowables (depending on the stress to density ratio). Furthermore, use of a stronger matrix (assuming all other properties were adequate) would also raise the allowables. Thus, the composite properties shown here are not the ultimate. They are representative of current properties, and there is further growth potential.

The two fiber contents were selected because they span the range of contents likely to be used in turbine blades. For example, at fiber contents below 30 volume percent in the critical section (blade cross section at which expected stress rupture life is shortest), the strength-to-density ratio would not be significantly better than those of the best superalloys. However, fiber contents between 30 and 40 volume percent in the critical section might permit a significant blade metal temperature advantage (depending on application) over the strongest current superalloys, such as MAR M200. And we calculate that the overall blade weights for these airfoil fiber contents may range from nearly equal to MAR M200 blade weight to only 10 percent greater than MAR M200 blade weights, for some current hollow blade designs. Thus, blades with these fiber contents could be suitable for use in aircraft engines where excess weight is a serious penalty. TFRS airfoil fiber contents will probably be 50 to 60 volume percent in land based turbines, according to Ref. 18. Although TFRS airfoils may outweight superalloy airfoils by as much as 50 percent in such an application, the extra weight may be acceptable because overall engine weight is a much less important factor in land based engines. Increased disc stress due to the greater blade weight would be a concern, but discs could also be made heavier and stronger to accommodate these disc stresses in land based turbines.

The thermal barrier and bond coatings, when applied, are assumed to be dead weight that must be supported by the TFRS or MAR M200 blade wall. Consequently, bulk temperature allowables must be decreased to account for the increased stress. To obtain a corrected stress-to-density ratio for use with Fig. 5, the TFRS stress-to-density ratio was multiplied by 1.09 and the MAR M200 stress-to-density ratio by 1.14 when the thermal barrier and bond coating thicknesses were assumed to be those listed in Table I.

Little is known regarding bulk and surface temperature allowables of zirconia and other thermal barrier coatings. However, to permit calculations, assumptions were made that these allowables were 2100K. It is recognized that these assumptions may be optimistic.

Results and Discussion

Composite Conductivity Values

Figure 6 depicts the conductivity experimental data obtained in this study.

The unreinforced matrix values indicate that FeCrAlY and ALLOY 3 have similar conductivities. Furthermore, their conductivities are similar to the typical matrix alloy defined earlier. Least square straight lines were drawn through the matrix data.

The composite conductivities are substantially higher than the matrix conductivities.

We calculated conductivity values for typical TFRS using the previously described equations and assumptions. The longitudinal conductivity values are plotted in Fig. 7, and the transverse conductivity values are plotted in Fig. 8. The TFRS conductivity experimental data are also reproduced on these figures. The measured conductivity of W/FeCrAlY and W/ALLOY 3 agree closely with the values predicted for typical TFRS. Subsequent references to TFRS conductivity are made with regard to the calculated curves. For comparison, the conductivity values of MAR M200, from Ref. 11, are also plotted.

According to Figs. 7 and 8 the transverse conductivity of typical TFRS airfoils (30 to 60 volume percent fibers), at typical airfoil metal temperatures, will be about 35 to 50 W/m-K. Longitudinal conductivities will be about 45 to 65 W/m-K. Typical superalloys, such as MAR M200, have conductivities of approximately 25 W/m-K at 1300K.

TFRS Turbine Blade Design Considerations

As indicated in Fig. 5, TFRS blades can have significant metal temperature advantages over conventional superalloy blades. And as shown in Figs. 7 and 8, TFRS clearly have higher thermal conductivity than a typical advanced superalloy. To evaluate the significance of these facts, one must consider which advanced turbine blade cooling configurations are likely to be used with TFRS.

TFRS will probably be used with impingement convection cooled blades (and possibly film-convection cooled blades containing few holes). Thus, it is fortunate that this design (Fig. 9) can have practical advantages over other designs. The following, taken mostly from Refs. 16, 19, and 20, may help to clarify this point. The advanced turbine blade cooling methods being considered by turbine designers are impingement convection, film-convection, full-film, transpiration, and liquid cooling. Impingement convection cooling, although the least efficient of these, is simple to achieve. It can involve no aerodynamic penalty, and allows blade designs with superior fatigue resistance relative to the other cooling methods. Thus, impingement convection cooled blades can be reliable, long life blades. Film-convection cooled blades are relatively simple in design, offer excellent cooling efficiency in the most critical regions of the blade, spill a relatively small amount of air in an aerodynamically detrimental way, but have lower fatigue resistance. On the other hand. full-film, transpiration, and liquid cooled designs offer very effective cooling, but they are subject to problems of complex construction, high aerodynamic penalty, increased susceptibility to oxidation damage, and poor fatigue resistance.

Impingement convection cooled blades are cooled by several mechanisms. Heat passes through the blade wall and leaves the blade via the cooling air exhaust. It also leaves by conduction along the span and flows into the disc. And it leaves by radiation to the environment. Since radiation is a function of the emissivity of the material surface which should be similar for TFRS and superalloys, subsequent discussion will not consider radiation.

Effect of conduction along the span. - Calculations similar to those performed in Ref. 21 indicate that metal temperatures near the root of a TFRS blade will be 5K to 10K cooler than those in a MAR M200 blade of similar geometry. This is due to the greater longitudinal conductivity of TFRS. Although disc temperatures might be raised slightly as a result, some turbine designs permit relatively easy disc cooling, Ref. 21. This property might be used to advantage in certain turbine designs; however, it may be a disadvantage in others. Also, greater longitudinal conductivity (combined with greater transverse conductivity) should result in lower blade metal temperature gradients. This should result in lower blade thermal stresses.

Effect of conduction through wall for blades without thermal barrier. - Turbine blade relative inlet gas temperature versus the coolant gas flow ratio is plotted in Fig. 10 for TFRS and MAR M200 blades with stress-to-density ratios of 12,000 N-m/kg and having the conductivities, metal bulk temperature, and surface temperature allowables described in Materials, Apparatus, and Procedure. At 0.06 coolant flow ratio, which is a reasonable value for an advanced engine, the 30 volume percent TFRS blade has a 150K gas temperature advantage over the MAR M200 blade. At 0.10 coolant flow, a high value currently used only in research engines, the 60 volume percent composite blade has a 250K advantage over the MAR M200 blade. Note also that the projected 60 volume percent TFRS turbine blade inlet gas temperature is over 2100K. Since the vane inlet total gas temperature is normally several hundred degrees higher than the turbine blade inlet relative gas temperature, use of TFRS blades could potentially permit near stoichiometric vane inlet gas temperatures. Because vane stresses are much lower than blade stresses, TFRS vanes can probably also be designed to permit such high vane inlet temperatures, assuming other problems of oxidation, fatigue, toughness, etc., can be overcome.

In some applications it may be more desirable to hold gas temperature constant and reduce coolant flow requirements. For instance, this might be done by substituting TFRS blades for superalloy blades in a current engine. In such cases the reduction in coolant flow could be considerable. Figure 10 indicates that if MAR M200 and a 30 volume percent TFRS blade were both used at 1765K (0.06 coolant flow for MAR M200) the coolant/gas flow ratio required by the TFRS would be 0.033, a 45 percent reduction in the cooling air flow needed. Using the 60 volume percent TFRS blade at 1800K (0.026 coolant/gas flow ratio) would result in a 65 percent reduction relative to the MAR M200 blade (0.074 coolant/gas flow ratio).

A third way to take advantage of TFRS blades would be to keep inlet temperature and cooling air flow the same as that of the superalloy blade. This would result in much lower TFRS blade metal temperature and presumably a longer blade life. Even a small, 25K to 50K, decrease in metal temperature could cause a many fold increase in stress rupture life for the TFRS according to Eqs. (9) through (13). However, stress-rupture life is not the only criterion for long blade life. Other life limiting factors, such as fatigue or corrosion, may limit blade life. Thus, TFRS blade life prediction which takes all of these factors into account would require a computer simulation beyond the scope of this study. Thus, we cannot say how much TFRS blade life would be increased simply by reducing metal temperature.

Effect of conduction through wall for blades with thermal barrier. - Figure 11 illustrates the effect of putting a thermal barrier coating on TFRS and MAR M200 blades both having a stress-to-density ratio of 12,000 N-m/kg (multiplied by the correction factor described previously). It is easy to see, comparing Figs. 10 and 11, that the thermal barrier coating is highly desirable. Moreover, Fig. 11 indicates that with thermal barriers applied, the TFRS blades have lost much of their temperature advantage over MAR M200 blades. This is mainly due to the fact that at higher temperatures the performance of the barrier coated composites is limited by the zirconia-nichrome interface temperature allowable of 1365K. This temperature is only slightly greater than the 60 volume percent TFRS bulk temperature allowable. Consequently, the thermal barrier coated 60 volume percent TFRS blade bulk temperature allowable is not reached at coolant flows above 0.005. Clearly, the coated TFRS cannot be used to their best advantage for blades with a 12,000 N-m/kg stress-to-density ratio due to the zirconia-nichrome interface temperature limitation Efficient use of the coated TFRS blade strengths may only be possible at higher stress-to-density ratios such as 16,000 to 20,000 N-m/kg. Only at these higher stress levels would the TFRS bulk temperature allowable be reached without exceeding the interface temperature allowable. Depending on fiber content, calculations show that coolant flow may still be under 0.04 for turbine inlet gas temperatures of 2100K at these higher stress-to-density ratios.

Although from the standpoint of heat transfer and blade inlet temperature, the thermal barrier coating works about as well on TFRS and superalloys, there is another consideration. That consideration is the thermal expansion difference between the coating and the turbine blade or vane material to which the coating is applied. The coefficient of thermal expansion for the zirconia coating is about 7×10^{-6} per degree K, Ref. 22. Fortunately, the thermal expansion of TFRS could be made to be similar to that of zirconia. According to our calculations, based on equations in Ref. 23, the TFRS coefficient of thermal expansion should range between 5×10^{-6} per degree K and 10×10^{-6} per degree K depending on fiber loading, cross ply configuration, matrix properties, and measurement direction. As yet unreported thermal expansion measurements made by the authors support these calculations. If need be, the thermal expansion of the TFRS might be tailored closely to that of the zirconia (or other similar thermal barrier coatings) by varying ply fiber contents and angles. Therefore, a thermal barrier coating could conceivably be more adherent on TFRS blades because of the potentially similar thermal expansions. Thus, durability of the thermal barrier coating could potentially be greater on TFRS blades than on conventional superalloys.

Summary of Results and Conclusions

The following major results and conclusions were obtained from an investigation to predict inlet gas temperatures potentially achievable with first generation TFRS turbine blades:

1. TFRS turbine blades may allow significantly higher inlet gas temperatures than are possible with conventional superalloy turbine blades. For instance, considering advanced impingement convection cooled blades operating at 40 atmospheres, a coolant flow of 0.06, and having a 12,000 N-m/kg stress-to-density ratio, 30 and 60 volume percent TFRS blades may permit 150K and 200K higher turbine inlet gas temperatures, respectively, than a similar MAR M200 blade.

2. At high coolant flows (about 0.10) a 60 volume percent TFRS blade could permit turbine inlet gas temperatures of over 2100K compared to only 1850K for a similar MAR M200 blade.

3. For a 12,000 N-m/kg stress-to-density ratio, 30 and 60 volume percent TFRS may allow coolant flow reductions of approximately 45 to 65 percent, respectively, compared to MAR M200 blades with the same stress-to-density ratio

and operating over the same gas temperature range (1500K to 1800K).

4. Thermal barrier coated TFRS blades could permit gas temperatures of 2100K at coolant flows below 0.04 assuming the thermal barrier survived the temperature.

5. The thermal expansion of TFRS can be made to closely match that of a zirconia thermal barrier or other similar coating, thus potentially improving adherence and durability of the coating.

6. At typical blade fiber contents and operating temperatures ranging from 1000K to 1400K, the transverse (through the wall) conductivity of TFRS blades will be approximately 35 to 50 W/m-K, and the longitudinal (spanwise) conductivity will be about 45 to 65 W/m-K. Typical superalloys have conductivities around 25 W/m-K at 1300K.

7. The root of TFRS blades may be cooler during operation than the root of a similar geometry superalloy blade because of the spanwise conductivity difference.

References

1. Signorelli, Robert A : "Review of Status and Potential of Tungsten-Wire - Superalloy Composites for Advanced Gas Turbine Engine Blades," NASA TM X-2599 [Sept. 1972]

2. Petrasek, Donald W.: "High-Temperature Strength of Refractory-Metal Wires and Consideration for Composite Applications," NASA TN D-6681 [Aug. 1972]

3. Winsa, Edward A., and Petrasek, Donald W.: "Factors Affecting the Miniature Izod Impact Strength of Tungsten-Fiber - Metal-Matrix Composites," NASA TN D-7393 [Oct. 1973]

4. Brentnall, W. D.: "Metal Matrix Composites for High Temperature Turbine Blades," TRW-ER-7790-F; TRW Inc., NADC 76225-30 [April 1976]

5. Barth, C. F., Blake, D. E., and Stelson, T. S.: "Cost Analysis of Advanced Turbine Blade Manufacturing Processes," ER-7930, TRW Corp.; NASA CR 135203 [Oct. 1977]

6. Brentnall, W. D., and [illegible]cz, D. J.: "Tungsten Wire - Nickel Base Alloy Composite Development," ER-7849, TRW Inc., NASA CR-135021 [March 1976]

7. Springer, G. S., and Tsai, S. W.: "Thermal Conductivities of Undirectional Materials," J. Compos. Mater. [1967] 166-173

8. Behrens, Ernst: "Thermal Conductivities of Composite Materials," J. Compos. Mater. [Jan. 1968] 2-17

9. Schulgasser, Kalman: "On the Conductivity of Fiber Reinforced Materials," J. Math. Phys. [Mar. 1976] 382-387

10. Dul'nev, G. N., Zarichnyak, Yu P., Karpinos, D. M., Klimenko, V. S., and Muratova, B. L.: "Thermal Conductivity of Composite Materials Made from Metal Fibers and Powders," Teplofiz Vys Temp 1100-1103 [Nov.-Dec. 1975] 1189-1192; High Temp. (Engl. Transl.) [May 1976]

11. High Temperature High Strength Nickel Base Alloys. 2nd Edition. The International Nickel Company of Canada, Ltd. Sudbury, Ontario, Canada [June 1968] 9, 12

12. Handbook of Chemistry and Physics, College Edition. 48th Edition. The Chemical Rubber Co., Cleveland, Ohio [1967] E-10

13. Logunov, A. V., and Kovalev, A. I.: "Experimental Investigation of the Thermophysical Properties of Tungsten-Rhenium Cast Alloys. 1. The W-5% Re Alloy," High Temp - High Pressures [1973] 625-633

14. Liebert, C. H., and Stepka, F. S.: "Potential Use of Ceramic Coating as a Thermal Insulation on Cooled Turbine Hardware," NASA TM X-3352 [Feb. 1976]

15. Stecura, Stephen: "Two-Layer Thermal Barrier Coating for Turbine Airfoils - Furnace and Burner Rig Test Results," NASA TM X-3425 [Sept. 1976]

16. Esgar, J. B., Colladay, R. S., and Kaufman, A.: "An Analysis of the Capabilities and Limitations of Turbine Air Cooling Methods," NASA TN D-5992 [Sept. 1970]

17. Lowell, C. E., and Deadmore, D. L.: "High Velocity Oxidation and Hot Corrosion Resistance of Some ODS Alloys," NASA TM X-73656 [April 1977]

18. Mazzi, P. J., Vandrunen, G., and Hakim, M. J.: "Powder Fabrication of Fiber-Reinforced Superalloy Turbine Blades," Advanced Fabrication Techniques in Powder Metallurgy and Their Economic Implications, AGARD-CP-200 [1976] Paper SC7

19. Moffitt, T. P., Stepka, F. S., and Rohlik, H. E.: "Summary of NASA Aerodynamic and Heat Transfer Studies in Turbine Vanes and Blades," NASA TM X-73518 [Dec. 1976]

20. Kaufmann, A.: "Analytical Study of Cooled Turbine Blades Considering Combined Steady-State and Transient Conditions," NASA TM X-1951 [Jan. 1970]

21. Gladden, Herbert J.: "Air Cooling of a Solid Integrally Cost Turbine Rotor for an Automotive Gas Turbine," NASA TM X-3471 [Jan. 1977]

22. Shaffer, Peter T. B.: No. 1 Materials Index, Plenum Press, New York [1964] 385-386

23. Ashton, J. E., Halpin, J. C., and Petit, P. H.: <u>Primer on Composite Materials: Analysis</u>, Technomic Publishing Co., Stanford, Conn. [1969] 88

Appendix - Symbols

A, B, and C	Larson-Miller parameters
D and E	reaction penetration parameters, m^2/hr and K
d	specimen thickness, m
h	gas heat transfer coefficient, W/m^2-K
K_I, K_{II}, K_{III}	coefficients of thermal conductivity for ceramic coating, bond coating, and blade metal wall, respectively, W/m-K
k	thermal conductivity coefficient, W/m-K
L_I, L_{II}, L_{III}	thickness of ceramic coating, bond coating, and blade metal wall, respectively, m
Q	heat flux, W
ρ	density, kg/m^3
R	radius of fiber, m
RP	depth of reaction penetration, m
S	specimen or reference cross section area, m^2
σ	stress, MPa
T	temperature, K
ΔT	temperature difference, K
$\overline{T}_I$, $\overline{T}_{II}$, $\overline{T}_{III}$	bulk (average) temperature of ceramic coating, bond coating, and blade metal wall, respectively, K
t	time, hr
V	volume fraction of the composite component
w	mass flow rate, kg/s

Subscripts:

c	coolant gas side
f	fiber property
g	inlet gas side
ℓ	longitudinal, i.e., measured parallel to fibers
m	matrix property
t	transverse, i.e., measured perpendicular to fibers
1	inlet gas-zirconia interface
2	zirconia-nichrome interface

3 nichrome-blade metal wall interface

4 blade metal wall-coolant gas interface

Table I. Assumed Values for Solving Equations (5) to (8)

$$h_c = 5.6\times10^4 \left(\frac{w_c}{w_g}\right)^{0.62} \ \mathrm{W/m^2\text{-}K}$$

$$h_g = 1.7\ T_g + 5260\ \mathrm{W/m^2\text{-}K}$$

$$K_I = 4.1\times10^{-4} \cdot \overline{T}_I + 0.46\ \mathrm{W/m\text{-}K}$$

$$K_{II} = 8.3\times10^{-3} \cdot \overline{T}_{II} + 6.7\ \mathrm{W/m\text{-}K}$$

$$K_{III}\ \text{(30 volume percent TFRS)} = 1.9\times10^{-2} \cdot \overline{T}_{III} + 12.4\ \mathrm{W/m\text{-}K}$$

$$K_{III}\ \text{(60 volume percent TFRS)} = 1.5\times10^{-2} \cdot \overline{T}_{III} + 32.0\ \mathrm{W/m\text{-}K}$$

$$K_{III}\ \text{(MAR M200)} = 1.71\times10^{-2} \cdot \overline{T}_{III} + 2.6\ \mathrm{W/m\text{-}K}$$

$$L_I = 0.13\times10^{-3}\ \mathrm{m}$$

$$L_{II} = 0.10\times10^{-3}\ \mathrm{m}$$

$$L_{III} = 1.3\times10^{-3}\ \mathrm{m}$$

T_g = varies from 1400K to 2100K

T_c = 811K

T_1, T_2, T_3, T_4 vary

Table II. Constants Used for Solving Equations (9) Through (14)

$$\left.\begin{array}{l} A_f = 4.0433 \\ B_f = -3.5841\times10^{-5} \\ C_f = 23.192 \\ A_m = 3.89 \\ B_m = -1.03\times10^{-4} \\ C_m = 20 \end{array}\right\} \text{These give stress in MPa}$$

$D = 584\ m^2/hr$

$E = -48{,}200K$

$\rho_f = 19{,}100\ kg/m^3$

$\rho_m = 7500\ kg/m^3$

RP (initial) = 3.05×10^{-6} m

$R = 0.1\times10^{-3}$ m or 0.4×10^{-3} m

t = 1000 hrs

T = 1200K to 1500K

$V_f = 0.30$ or 0.60

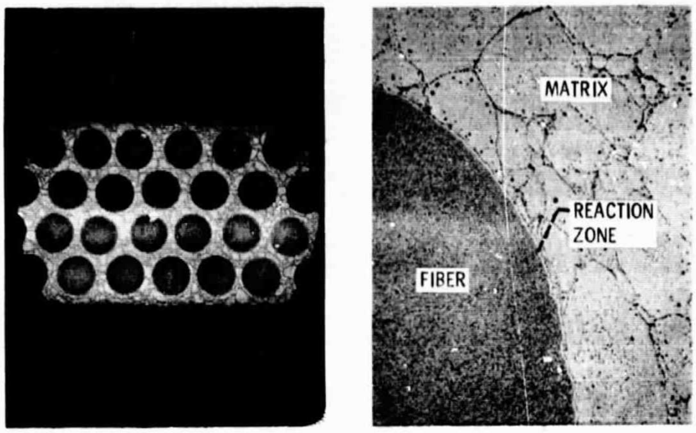

(a) 25 DIAMETERS MAGNIFICATION. (b) 500 DIAMETERS MAGNIFICATION.

Figure 1. - Photomicrograph of W-1 ThO_2/FeCrAlY sheet showing regular hexagonal fiber array and reaction zone caused by reaction penetration after exposing to fabrication temperatures of 1395 K for 1 hour. Fiber diameter, 0.038 cm.

ORIGINAL PAGE IS OF POOR QUALITY

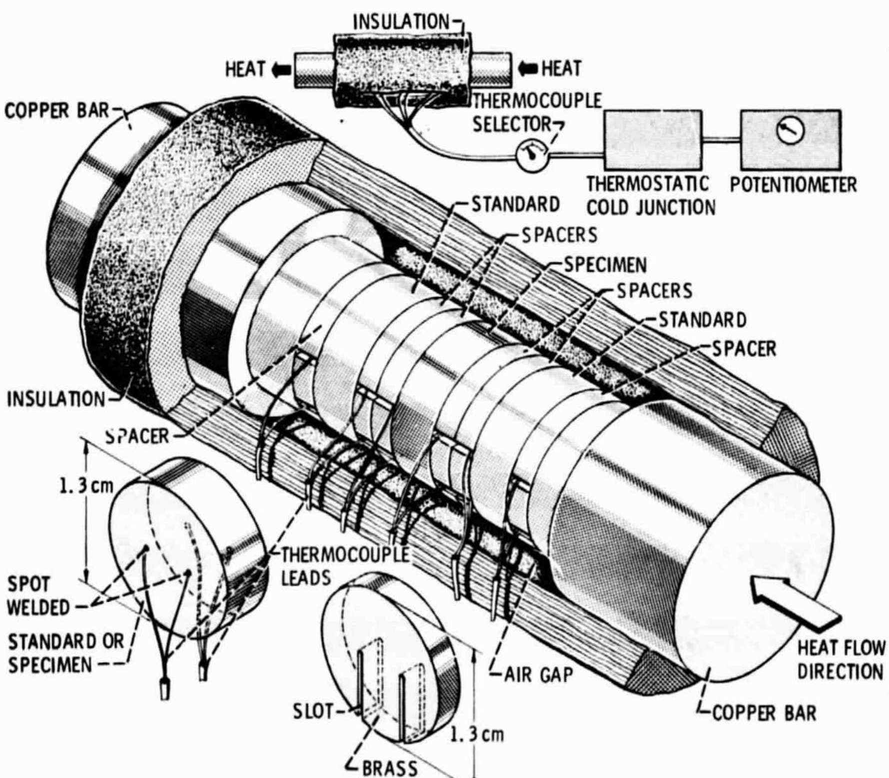

Figure 2. - Thermal conductivity measurement apparatus. Heat passes through standards and specimen between them. Precision thermocouple thermostatic cold junction and potentiometer used to determine temperatures.

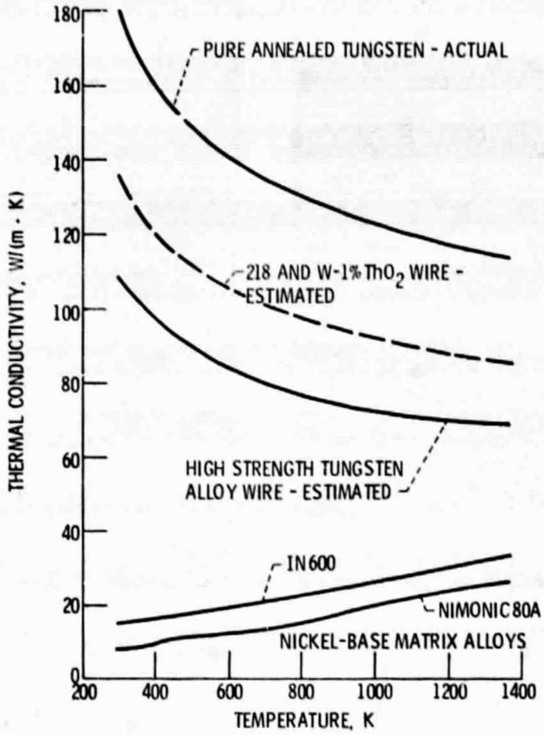

Figure 3. - Assumed thermal conductivities of TFRS fiber and matrix alloys. The 218 tungsten curve and middle of matrix band were assumed to be typical and used in calculations.

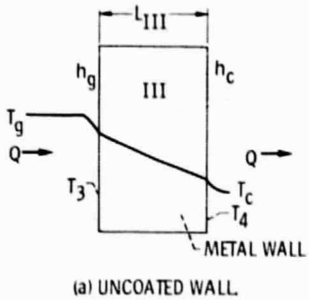

(a) UNCOATED WALL.

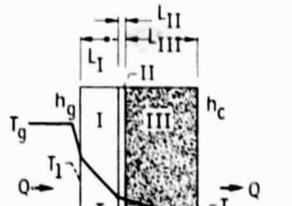

(b) THERMAL BARRIER COATED WALL.

Figure 4. - Sketch of hypothetical impingement cooled blade wall showing relationships among variables and parameters.

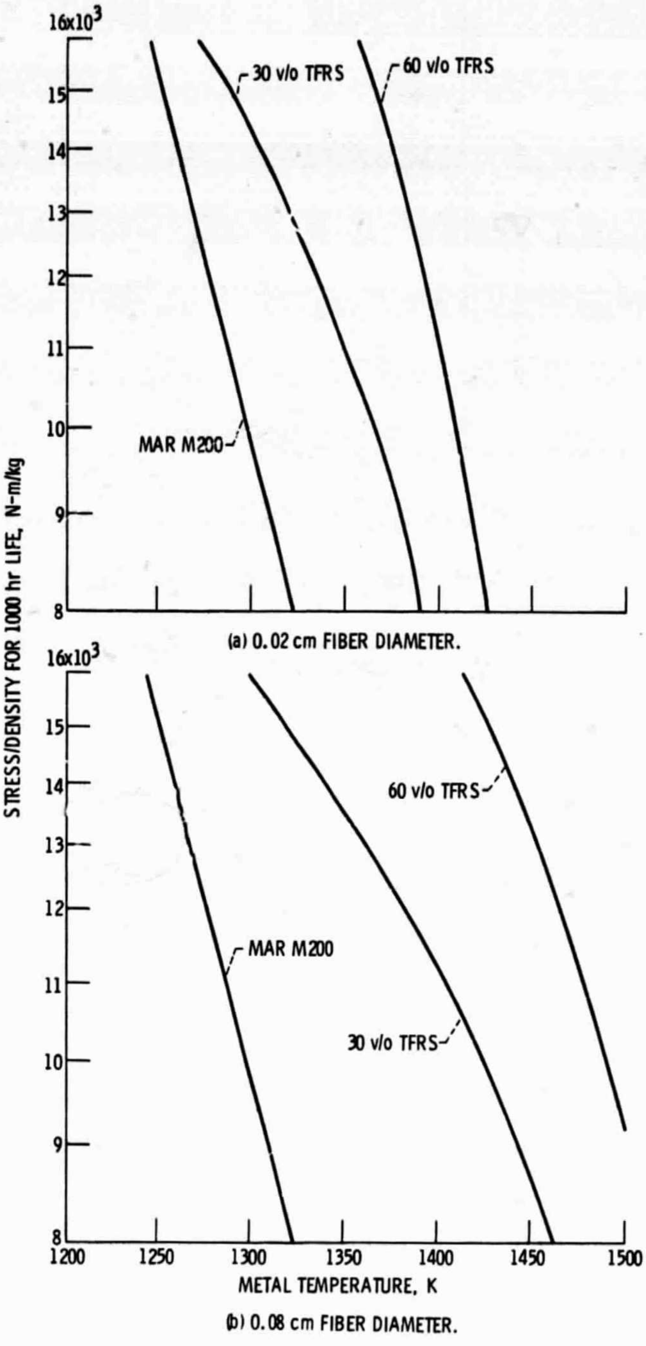

Figure 5. - Relationship between TFRS blade strength and metal temperature for TFRS having current strength properties (there is growth potential). Note that the advantage of TFRS over MAR M200 increases as stress-to-density decreases and as fiber diameter increases.

E-9429

ORIGINAL PAGE IS
OF POOR QUALITY

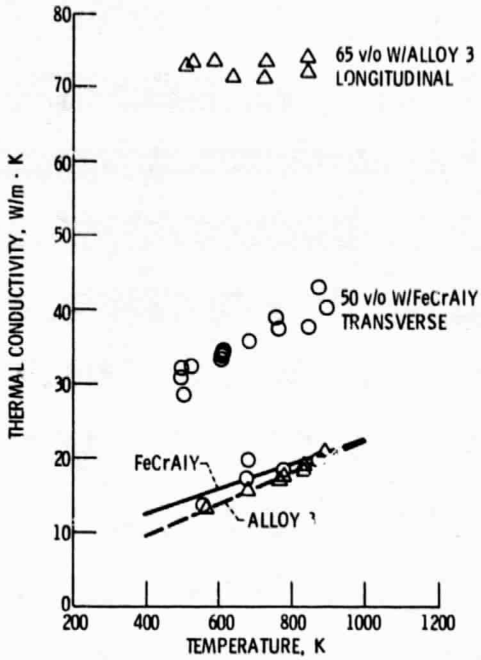

Figure 6. - Measured thermal conductivity of TFRS composites and matrix alloys.

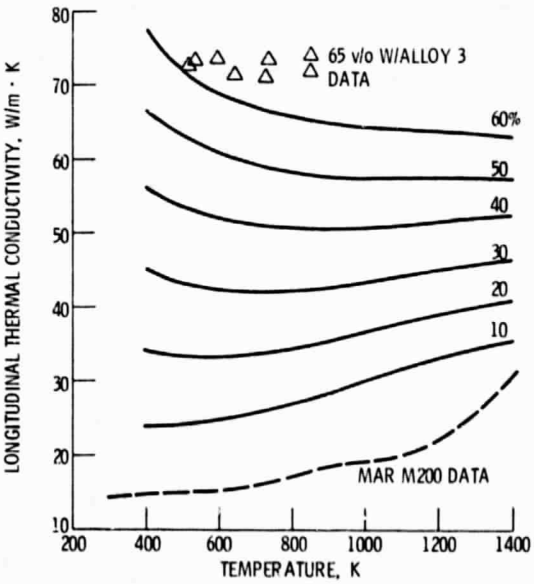

Figure 7. - Calculated longitudinal (spanwise) conductivities of typical TFRS.

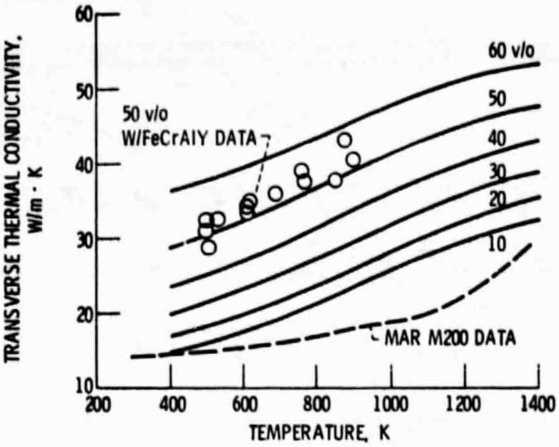

Figure 8. - Calculated transverse (through the wall) conductivities of typical TFRS. Comparison with figure 7 shows longitudinal conductivity to be greater than transverse conductivity.

E-1429

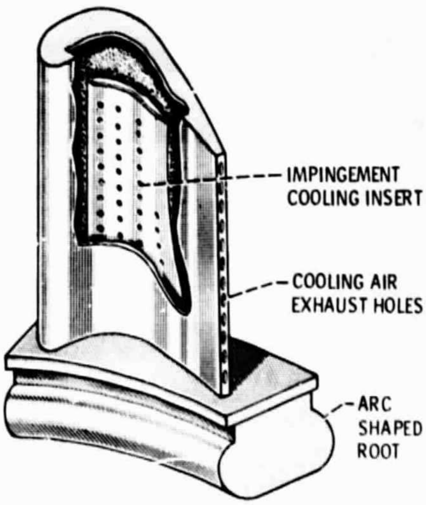

ORIGINAL PAGE IS OF POOR QUALITY

Figure 9. - Schematic of impingement convection cooled blade. The arc shaped root attachment may be required on TFRS blades.

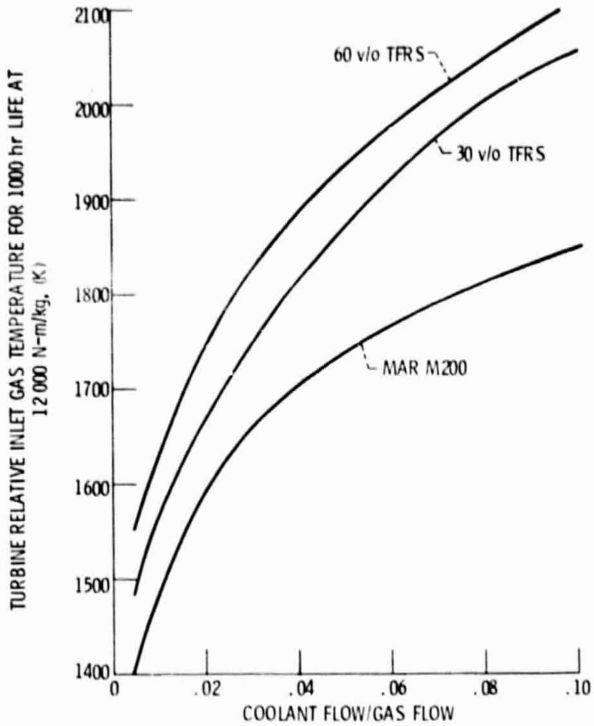

Figure 10. - Turbine blade inlet relative gas temperature as a function of coolant/gas flow ratio for hypothetical advanced engine operating at 40 atmospheres pressure. Blades assumed to be impingement convection cooled with a coolant temperature of 811 K.

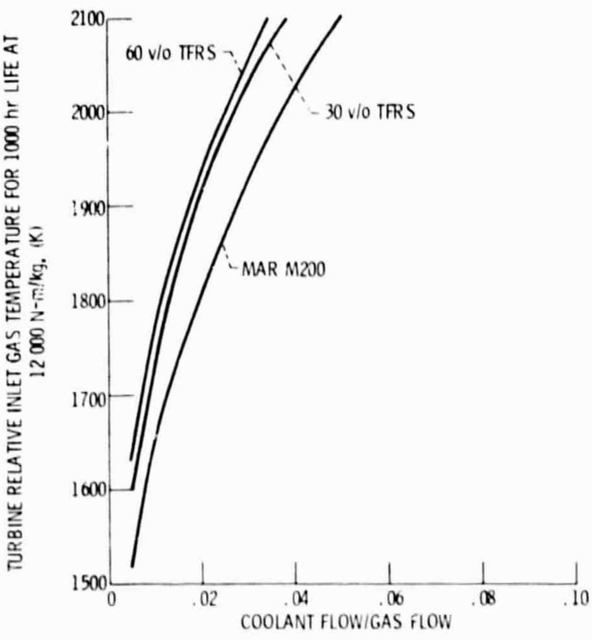

Figure 11. - Thermal barrier coated turbine blade inlet relative gas temperature as a function coolant/gas flow ratio for hypothetical advanced engine operating at 40 atmospheres pressure. Blades assumed to be impingement convection coated with a coolant temperature of 811 K.

NASA-Lewis-Com'l